# A pivotal role for a conserved bulky residue at the α1-helix of the αI integrin domain in ligand binding

Received for publication, April 9, 2017, and in revised form, October 12, 2017 Published, Papers in Press, October 27, 2017, DOI 10.1074/jbc.M117.790519

**Zhengli Wang**[‡], **Aye Myat Myat Thinn**[‡§], **and Jieqing Zhu**[‡§1]

*From the* [‡]*Blood Research Institute, BloodCenter of Wisconsin, Milwaukee, Wisconsin 53226 and the* [§]*Department of Biochemistry, Medical College of Wisconsin, Milwaukee, Wisconsin 53226*

Edited by Alex Toker

**The ligand-binding βI and αI domains of integrin are the best-studied von Willebrand factor A domains undergoing significant conformational changes for affinity regulation. In both βI and αI domains, the α1- and α7-helixes work in concert to shift the metal-ion–dependent adhesion site between the resting and active states. An absolutely conserved Gly in the middle of the α1-helix of βI helps maintain the resting βI conformation, whereas the homologous position in the αI α1-helix contains a conserved Phe. A functional role of this Phe is structurally unpredictable. Using $\alpha_L\beta_2$ integrin as a model, we found that the residue volume at the Phe position in the α1-helix is critical for $\alpha_L\beta_2$ activation because trimming the Phe by small amino acid substitutions abolished $\alpha_L\beta_2$ binding with soluble and immobilized intercellular cell adhesion molecule 1. Similar results were obtained for $\alpha_M\beta_2$ integrin. Our experimental and molecular dynamics simulation data suggested that the bulky Phe acts as a pawl that stabilizes the downward ratchet-like movement of β6-α7 loop and α7-helix, required for high-affinity ligand binding. This mechanism may apply to other von Willebrand factor A domains undergoing large conformational changes. We further demonstrated that the conformational cross-talk between $\alpha_L$ αI and $\beta_2$ βI could be uncoupled because the $\beta_2$ extension and headpiece opening could occur independently of the αI activation. Reciprocally, the αI activation does not inevitably lead to the conformational changes of the $\beta_2$ subunit. Such loose linkage between the αI and βI is attributed to the αI flexibility and could accommodate the $\alpha_L\beta_2$-mediated rolling adhesion of leukocytes.**

Integrins are cell adhesion molecules that transmit both the mechanical and chemical signals into and out of the cells and thus allow the cells to communicate with their surroundings (1–4). The different combinations of 18 α and 8 β subunits lead to 24 integrin α/β heterodimers that play important roles in diverse physiological and pathological conditions such as hemostasis, development, immune responses, thrombosis, inflammation, and cancer (1). All the β integrin subunits consist of 10 subdomains, ranking from the N terminus to the C terminus are PSI (plexin, semaphorin, and integrin), hybrid, I (inserted), integrin epidermal growth factor (I-EGF)[2] 1–4, β-tail, transmembrane, and cytoplasmic tail domains (Fig. 1, *A–F*). All the α integrin subunits are composed of seven subdomains, namely β-propeller, thigh, genu, calf-1, calf-2, transmembrane, and cytoplasmic tail (Fig. 1, *A–F*). In addition, half of the α subunits including the leukocyte-specific integrins $\alpha_L$ and $\alpha_M$ contain an extra αI domain that is inserted into the β-propeller domain (Fig. 1, *D–F*). For integrins without the αI domain, the β-propeller and the βI domain form the ligand-binding site at the top of their interface (Fig. 1, *A–C*), whereas the αI domain is solely responsible for binding ligands when it is present in an α subunit (Fig. 1, *D–F*). It has been demonstrated that the conserved Glu residue at the αI C terminus acts as an internal ligand for the βI domain (Fig. 1*F*) (5). EM, crystallography, small-angle X-ray scattering, and mutagenesis studies have revealed at least three conformational states of integrin: bent (Fig. 1, *A* and *D*), extended with closed headpiece (Fig. 1, *B* and *E*), and extended with open headpiece (Fig. 1, *C* and *F*), which have been proposed to represent the inactive, intermediate, and active integrin conformations, respectively (5). Such a bent-to-extended global conformational transition can be triggered from the ligand-binding head region and transmit in the outside-in direction or propagated from the cytoplasmic tail and transmit in the inside-out direction. How the wave of conformational change is relayed mechanically across the tandem multiple domains of integrin has been an active area of research in the last decades (6–10).

Integrin global conformational rearrangements are triggered by the local structural changes (11), which have been very well-defined for the αI and βI domains by the crystal structures (12–17). The αI and βI domains (also known as A domains) are structural homologs that belong to the large von Willebrand factor A (VWA) domain superfamily, which is widespread in the eukaryotes, bacteria, and viruses and perhaps beyond them (18). Both αI and βI domains contain a metal ion-dependent adhesion site (MIDAS) defined by a signature Asp-Xaa-Ser-Xaa-Ser (D*X*S*X*S) motif (Fig. 1*G*), which is connected to the N terminus of an α1-helix and also is seen in many other VWA

This work was supported by Grants HL122985 and HL131836 (to J. Zhu) from the NHLBI, National Institutes of Health. The authors declare that they have no conflicts of interest with the contents of this article. The content is solely the responsibility of the authors and does not necessarily represent the official views of the National Institutes of Health.

[1] To whom correspondence should be addressed: Blood Research Institute, BloodCenter of Wisconsin, 8727 Watertown Plank Rd., Milwaukee, WI 53226. Tel.: 414-937-3867; Fax: 414-937-6284; E-mail: Jieqing.Zhu@bcw.edu.

[2] The abbreviations used are: I-EGF, integrin epidermal growth factor; VWA, von Willebrand factor A; MIDAS, metal ion-dependent adhesion site; ICAM-1, intercellular adhesion molecular 1; ADMIDAS, adjacent to MIDAS; APC, allophycocyanin; MD, molecular dynamics; RMSD, root mean square deviation; RMSF, root mean square fluctuation; TRAP, thrombospondin repeat anonymous protein; PDB, Protein Data Bank.



© 2017 by The American Society for Biochemistry and Molecular Biology, Inc. Published in the U.S.A.

domains (Fig. 1*J*). In addition, the βI domains have two additional metal ion-binding sites flanking the MIDAS, namely adjacent to MIDAS (ADMIDAS) and synergetic metal ion-binding sites (Fig. 1*H*). Both αI and βI domains can shift between two conformations defined as the closed inactive and the open active states. In the active state, the β1-α1 loop moves toward the MIDAS, increasing its potential for binding ligands (Fig. 1, *H* and *I*). For βI domain, this is accompanied by a bent-to-straight structural transition, resulting in an inward movement of the α1/α1′-helix (Fig. 1*H*), whereas for αI domain, it is associated with only a swung-in motion of the N terminus of α1-helix (Fig. 1*I*). For both βI and αI domains, such conformational changes of α1/(α1′)-helix are linked with a downward displacement of β6-α7 loop and α7-helix, leading to hybrid domain swinging out (Fig. 1, *C*, *F*, and *H*) or the engagement of αI and βI domain via an internal ligand at the C terminus of α7-helix (Fig. 1, *F* and *I*). In our recent studies, we defined the role of an absolutely conserved Gly residue at the α1/α1′-helix (Fig. 1*H*), which is critical in maintaining the inactive conformation of βI domains of $\beta_1$, $\beta_2$, and $\beta_3$ integrins (19). Interestingly, a conserved Phe is present at a homologous position of the αI α1-helix among all the αI-containing integrins (Fig. 1, *G* and *I*). The equivalent Phe is also seen in the α1-helix of many VWA domains other than integrin (Fig. 1*J*). We speculated that such a conserved Phe residue could be important for the activation of αI domains.

In this study, we tested our above-mentioned hypothesis on $\alpha_L\beta_2$ integrin, given that the activation assay of $\alpha_L\beta_2$ has been very well-established and the high-resolution crystal structures of the $\alpha_L$ αI domain are available in both closed and open states (15, 19–21). The $\alpha_L\beta_2$ integrin binds ligand intercellular adhesion molecule 1 (ICAM-1) and plays important roles in leukocyte adhesion and migration during the immune responses (5). To investigate a potential structural role of the conserved Phe of the αI α1-helix in regulating the activity of $\alpha_L\beta_2$ integrin, we performed the soluble ICAM-1 binding, cell adhesion, and the conformation-specific mAb-binding assays. Our results revealed an unexpected function of the Phe residue in $\alpha_L\beta_2$ activation, which may be generalized to all the integrin αI domains or other related VWA domains that couple large-scale conformational changes to activation and ligand binding.

## Results

### *A bulky residue in the mid position of α1-helix of $\alpha_L$ αI domain is critical for ligand binding*

A hallmark structural change of αI domain in the transition from the low to the high-affinity state is the inward movement of the N terminus of α1-helix and the piston-like movement of the entire α7-helix (Fig. 1, *E*, *F*, and *I*). Structural superimposition of the active conformation onto the resting conformation of the $\alpha_L$ αI domain shows steric clashes between the N-terminal interfacial residues of α1-helix and α7-helix (Fig. 2*A*), indicating that these helixes should mechanically work in concert to avoid the collisions. Interestingly, the invariant phenylalanine residue $\alpha_L$-Phe-153 at the middle of α1-helix in the active position has no van der Waals overlaps with the α7-helix in the resting position (Fig. 2*A*). To test whether the conserved $\alpha_L$-Phe-153 is important for the activation of $\alpha_L$ integrin, we mutated it to Gly, Ala, Val, Leu, Met, Tyr, and Trp, respectively, ranging from the slimmest Gly to the bulkiest Trp (Fig. 2*B*). The activation of $\alpha_L\beta_2$ integrin was assessed by the ICAM-1-binding assay in the presence of the universal integrin activator $Mn^{2+}$. Remarkably, the $\alpha_L$-F153G and $\alpha_L$-F153A mutations almost completely abrogated $Mn^{2+}$-induced ICAM-1 binding to HEK293FT cells expressing $\alpha_L\beta_2$ integrin (Fig. 2*C*). Remarkably, the level of ICAM-1 binding correlated well with the side chain volumes of the substituted amino acids for $\alpha_L$-Phe-153, *i.e.* Gly = Ala < Val < Met < Leu = Phe = Tyr < Trp (Fig. 2*C*). As a comparison, the $\alpha_L$-Glu-146 and $\alpha_L$-Lys-149 were mutated to Ala. These residues show steric clashes with the α7-helix Phe-292 when overlapping their high-affinity conformation with the low-affinity conformation of α7-helix (Fig. 2*A*). As expected, both $\alpha_L$-E146A and $\alpha_L$-K149A mutations greatly dampened $Mn^{2+}$-induced ICAM-1 binding, but to a lesser extent compared with the $\alpha_L$-F153A mutation (Fig. 2*D*). Interestingly, the $\alpha_L$-F147A and $\alpha_L$-L151A mutations, located at the opposite side of the α1- and α7-helix interface (Fig. 2*A*), also decreased ICAM-1 binding (Fig. 2*D*). By contrast, the $\alpha_L$-K160A mutation at the bottom of α1-helix had no effect on $Mn^{2+}$-induced ICAM-1 binding of $\alpha_L\beta_2$ integrin (Fig. 2, *A* and *D*). Most of the mutations had little effect on the $\alpha_L\beta_2$ cell surface expression except the Leu substitution decreased the expression by ~50% (Fig. 2, *C* and *D*). In addition, the $\alpha_L$-F153I mutation completely abolished $\alpha_L\beta_2$ cell surface expression probably because the position of $\alpha_L$-Phe-153 cannot accommodate an Ile residue because all the Ile rotamers show severe steric clashes with the surrounding residues when mutated *in silico* (data not shown). These data demonstrated that a bulky amino acid in the mid α1-helix is critical for the high-affinity ligand binding of αI domain. In addition, the N-terminal residues of α1-helix also contribute to the high-affinity conformation of α1-helix.

### *Mutations that lock the high-affinity conformation of α7-helix of αI domain counteract the inactivating effect of the α1-helix Phe-153 mutation*

It has been shown that the downward movement of the α7-helix is important for the activation of αI domain (15, 22, 23). We speculated that the inactivating effect of the $\alpha_L$-F153G or F153A mutation could be due to the destabilization of the downward movement of α7-helix. In line with this possibility, enforcing the downward movement of α7-helix, for example by mutations, may rescue the inactivating effect of the $\alpha_L$-F153 mutations. This hypothesis was tested using four activating mutations of $\alpha_L\beta_2$ integrin. The $\beta_2$-G128A/G129T mutation (Fig. 3*A*) renders $\alpha_L\beta_2$ activation by facilitating the active conformation of βI domain α1-helix (19). The $\alpha_L$-F265S mutation induces the downward movement of αI α7-helix by facilitating the movement of the β5-α6 loop (Fig. 3, *A* and *B*) (24), whereas the $\alpha_L$-K287C/K294C mutation directly stabilizes the downward movement of the β6-α7 loop and α7-helix of αI domain by forming a disulfide bond (Fig. 3, *A* and *C*) (15). The $\alpha_L$-GFFKR/GAAKR (FFAA) mutation renders $\alpha_L\beta_2$ constitutively active by disrupting the α-β cytoplasmic association, which mimics the inside-out activation of integrin (Fig. 3*A*) (25). As shown in Fig. 3*D*, the presence of the $\beta_2$-G128A/G129T

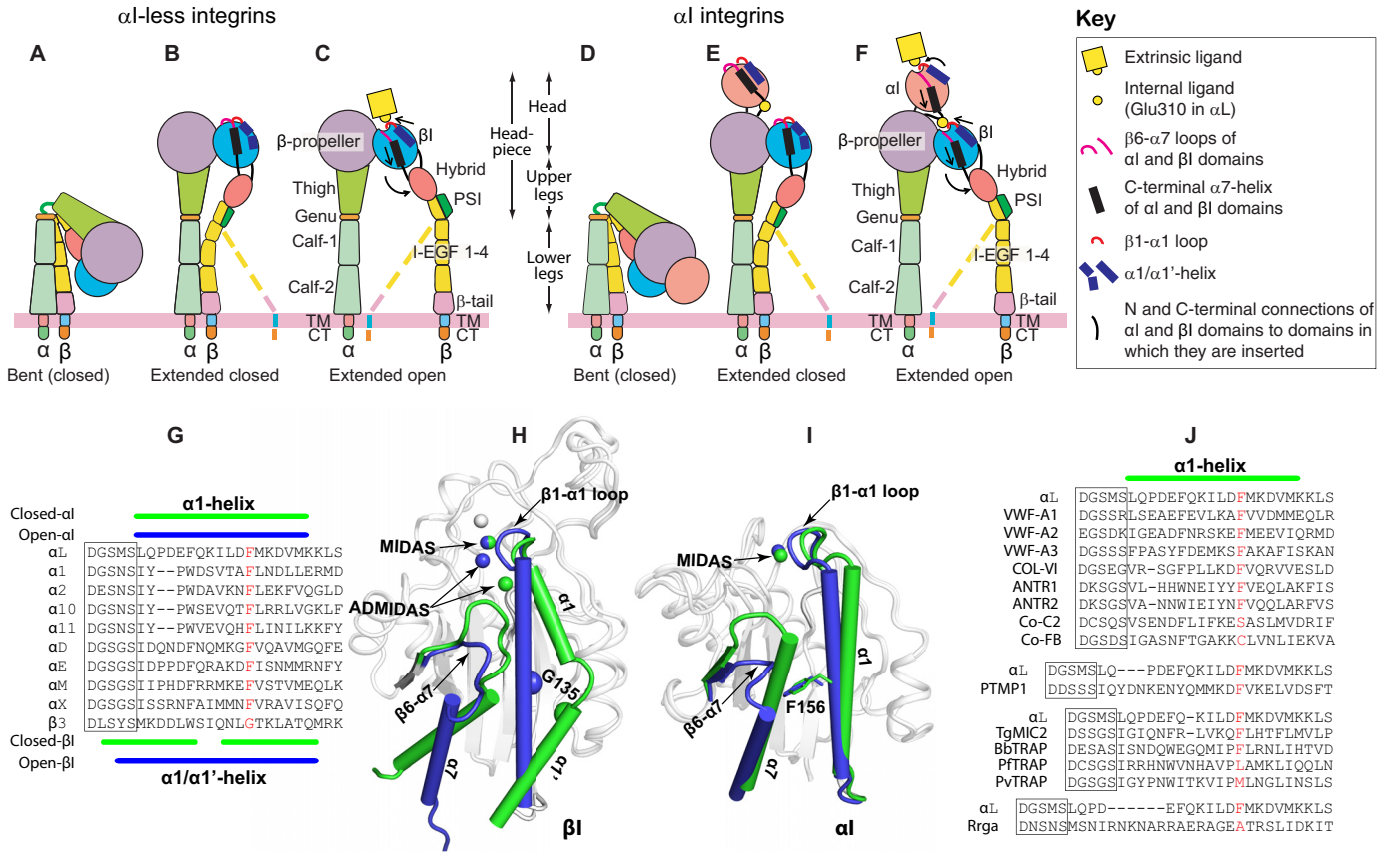


**Figure 1. Integrin domain organization and the allosteric signal relay in the global and local conformational changes.** *A–C*, the three major conformational states of integrins without the αI domain. *D–F*, the three major conformational states of integrins with an αI domain inserted into the β-propeller domain of α subunit. The local conformational changes of the α1-helix, α7-helix, and the β subunit hybrid domain were indicated by *arrows*. Potential intermediate conformations of β subunit are shown as *dashed lines*. *G*, sequence alignment of the α1-helixes of the αI domains. The α1/α1′-helix sequence of the $\beta_3$ integrin βI domain was shown for comparison. *H*, structure comparison of the $\beta_3$ βI domain in the closed (PDB code 3T3P) and open conformations (PDB code 2VDR). *I*, structure comparison of the $\alpha_M$ αI domain in the closed (PDB code 1JLM) and open conformations (PDB code 1IDO). The closed and open conformations of α1/α1′-helix and α7-helix are shown in *green* and *blue*, respectively. Metal ions of the MIDAS and ADMIDAS are shown as *spheres*. $\beta_3$-Gly-135 is shown as a Cα *sphere*. The $\alpha_M$-Phe-156, equivalent to $\alpha_L$-Phe-153, is shown as *sticks*. *J*, structure-based sequence alignment of the α1-helix from the selected VWA domains. The D*X*S*X*S motifs of the MIDAS are *boxed*. Residues that are equivalent to $\alpha_L$-Phe-153 are shown in *red*.

mutation did not rescue the inactivating effect of $\alpha_L$-F153G and $\alpha_L$-F153A. However, compared with the $\beta_2$ wild type (Fig. 2*C*), the requirement of residue size at the position of $\alpha_L$-153 for $Mn^{2+}$-induced ICAM-1 binding was weakened by the $\beta_2$-G128A/G129T mutation (Fig. 3*D*). With the $\beta_2$-G128A/G129T mutation, even the $\alpha_L$-F153V rendered the same level of ICAM-1 binding as the $\alpha_L$ wild type in the presence of $Mn^{2+}$ but not $Ca^{2+}/Mg^{2+}$ (Fig. 3*D*). Consistently, the bulkiest amino acid Trp further enhanced the ICAM-1 binding at both metal ion conditions (Fig. 3*D*). There was ~20% decrease of the $\alpha_L\beta_2$ cell surface expression because of these mutations (Fig. 3*D*). In sharp contrast, both the $\alpha_L$-F265S and $\alpha_L$-K287C/K294C mutations completely rescued the inactivating effect of $\alpha_L$-F153A (Fig. 3*E*). Interestingly, the $\alpha_L$-F153A mutation even enhanced the activating effect of $\alpha_L$-K287C/K294C (Fig. 3*E*). Although the $\alpha_L$-FFAA mutation induced the similar level of $\alpha_L\beta_2$ activation as the $\alpha_L$-F265S and $\alpha_L$-K287C/K294C mutations, it failed to rescue the inactivating effect of $\alpha_L$-F153A (Fig. 3*E*). All of these mutations clearly decreased the cell surface expression of $\alpha_L\beta_2$ integrin (Fig. 3*E*). These data suggest that the bulky $\alpha_L$-Phe-153 of α1-helix is critical for stabilizing the downward displacement of α7-helix, required for the high affinity ligand binding of $\alpha_L\beta_2$ integrin.

### *The $\alpha_L$-F153A mutation has little effect on the overall conformational change of $\beta_2$ integrin*

Integrin activation is associated with the long-range conformational rearrangements that are relayed among the connecting domains (5). Such conformational changes on the cell surface can be measured by the exposure of epitopes that are masked in the bent inactive conformation (26). Next, we asked whether the inactivating $\alpha_L$-F153A mutation could affect the global conformational change of $\alpha_L\beta_2$ integrin. Two conformation-specific mAbs were used to report the conformational states of $\alpha_L\beta_2$ integrin. The mAb m24 binds to the $\beta_2$ βI domain and is specific to the open headpiece conformation (27) (Fig. 3*A*). The mAb KIM127 binds to the I-EGF2 domain of $\beta_2$ leg and is specific to the extended conformation of $\beta_2$ (28, 29) (Fig. 3*A*). $Mn^{2+}$ induced the binding of both m24 and KIM127 to the $\alpha_L\beta_2$ integrin expressed in HEK293FT cells (Fig. 4, *A* and *B*), indicating the headpiece opening and leg extension. The inactivating mutations $\alpha_L$-K149A and $\alpha_L$-F153A decreased ICAM-1 binding by more than 90% (Fig. 2*B*). By contrast, these mutations had no effect on $Mn^{2+}$-induced binding of m24 (Fig. 4*A*) or KIM127 (Fig. 4*B*) binding to the $\beta_2$ wild type. The $\alpha_L$-F153W mutation had no obvious effect on the binding of

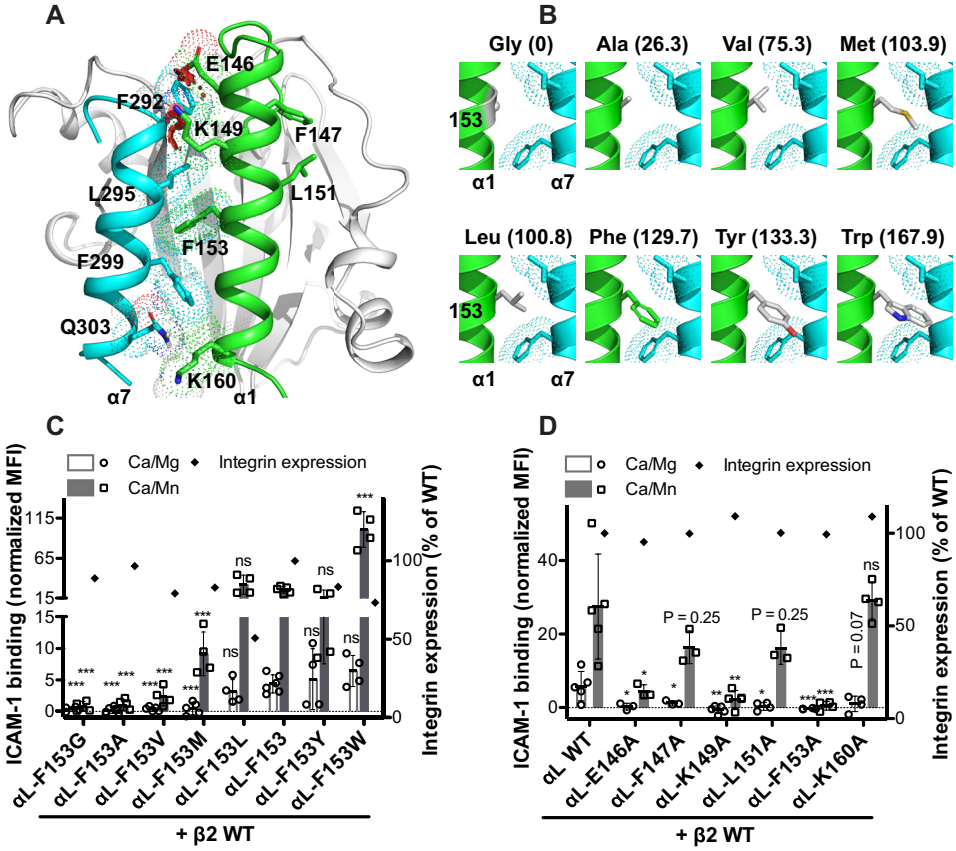


**Figure 2. Effect of mutations in the α1-helix of αI domain on $\alpha_L\beta_2$ ligand binding.** *A*, conformations of the α1-helix and α7-helix of $\alpha_L$ αI domain. The crystal structures of the $\alpha_L$ αI domain in the closed (PDB code 1ZOP) and the open (PDB code 1MQA) conformations are superimposed, and the conformations of α1-helix in the open state (in *green*) and α7-helix in the closed state (in *cyan*) are shown. The residues at the interface of α1-helix and α7-helix are shown as *sticks* with *dotted surfaces*. The van der Waals overlaps (steric clashes) between the interfacial residues are indicated as *red disks*. *B*, structural comparison of the amino acids used for the substitution of $\alpha_L$-Phe-153. The $\alpha_L$-Phe-153 was mutated *in silico* using PyMOL. The rotamers that have minimal or no steric clashes with their surroundings were selected. The volumes (Å$^3$) of amino acid side chains occupying in protein interiors are shown in *parentheses* (66). *C* and *D*, ICAM-1 binding of HEK293FT cells transfected with $\beta_2$ WT and $\alpha_L$ containing indicated α1-helix mutations. The ICAM-1 binding was measured by flow cytometry in the presence of 1 mM $Ca^{2+}/Mg^{2+}$ (*Ca/Mg*) or 0.2 mM $Ca^{2+}$ plus 2 mM $Mn^{2+}$ (*Ca/Mn*) and presented as the MFI normalized to integrin expression. The data are means ± S.D. ($n \geq 3$). Two-tailed *t* tests were used to compare the wild type and the mutants in the same conditions. *, $p < 0.05$; **, $p < 0.01$; ***, $p < 0.001$; *ns*, $p > 0.05$. Only the mean values are shown for the integrin expression.

both mAbs compared with the wild type (Fig. 4, *A* and *B*). The activating $\alpha_L$-FFAA mutation, which mimics the integrin inside-out activation, induced spontaneous binding of m24 and KIM127, which was further enhanced by $Mn^{2+}$ (Fig. 4, *A* and *B*). Although the $\alpha_L$-F153A mutation significantly reduced the binding of both mAbs when combined with the $\alpha_L$-FFAA mutation, it only decreased the mAb binding by 14 or 18% (Fig. 4, *A* and *B*), which is in sharp contrast with the almost 100% decrease of ICAM-1 binding (Fig. 3*E*). In line with these findings, neither $\alpha_L$-K149A nor $\alpha_L$-F153A affected the binding of m24 and KIM127 in the presence of the activating mutant $\beta_2$-G128A/G129T that stabilizes the active conformation of βI α1-helix (Fig. 4, *A* and *B*). As seen in our previous study on $\beta_1$ and $\beta_3$ integrins (19), the $\beta_2$-G128A/G129T mutation increased the binding of both m24 and KIM127 compared with the wild type (Fig. 4). These data demonstrated that the inactivating mutations at the αI α1-helix had little effect on the headpiece opening and extension induced by the signals of outside-in or inside-out activation. This is consistent with the previous study showing that locking the αI domain in a high-affinity conformation by the $\alpha_L$-K287C/K294C mutation did not induce the binding of m24 or KIM127 (22). Thus, the conformational changes between the αI and the $\beta_2$ subunit can be uncoupled during the transmission of conformational changes.

To further define the structure requirement for $\beta_2$ headpiece opening and extension, we introduced a $\beta_2$-KKGG mutation at the α1-helix of βI domain (Fig. 3*A*). This mutation has been shown in our previous study to dramatically reduced ICAM-1 binding to $\alpha_L\beta_2$ integrin by stabilizing the inactive conformation of α1-helix (19). In opposition to the $\beta_2$-G128A/G129T mutation of α1-helix, the $\beta_2$-KKGG mutation greatly impaired the binding of m24 and KIM127 when co-expressed with the $\alpha_L$ wild type (Fig. 4). Moreover, it reduced the m24 binding by more than 90% (Fig. 4*A*), and the KIM127 binding by more than 50% (Fig. 4*B*), even when combined with the activating $\alpha_L$-FFAA mutation. These data clearly demonstrated that the active conformation of βI α1-helix; *i.e.* the inward movement toward the MIDAS (Fig. 1, *F* and *H*), is essential for $\beta_2$ headpiece opening and extension.

### *The $\alpha_L$-F153A mutation abolishes $\alpha_L\beta_2$-mediated cell adhesion on immobilized ICAM-1*

Having established the critical role of $\alpha_L$-F153 in the binding of $\alpha_L\beta_2$ integrin to soluble ICAM-1, we asked whether it is also

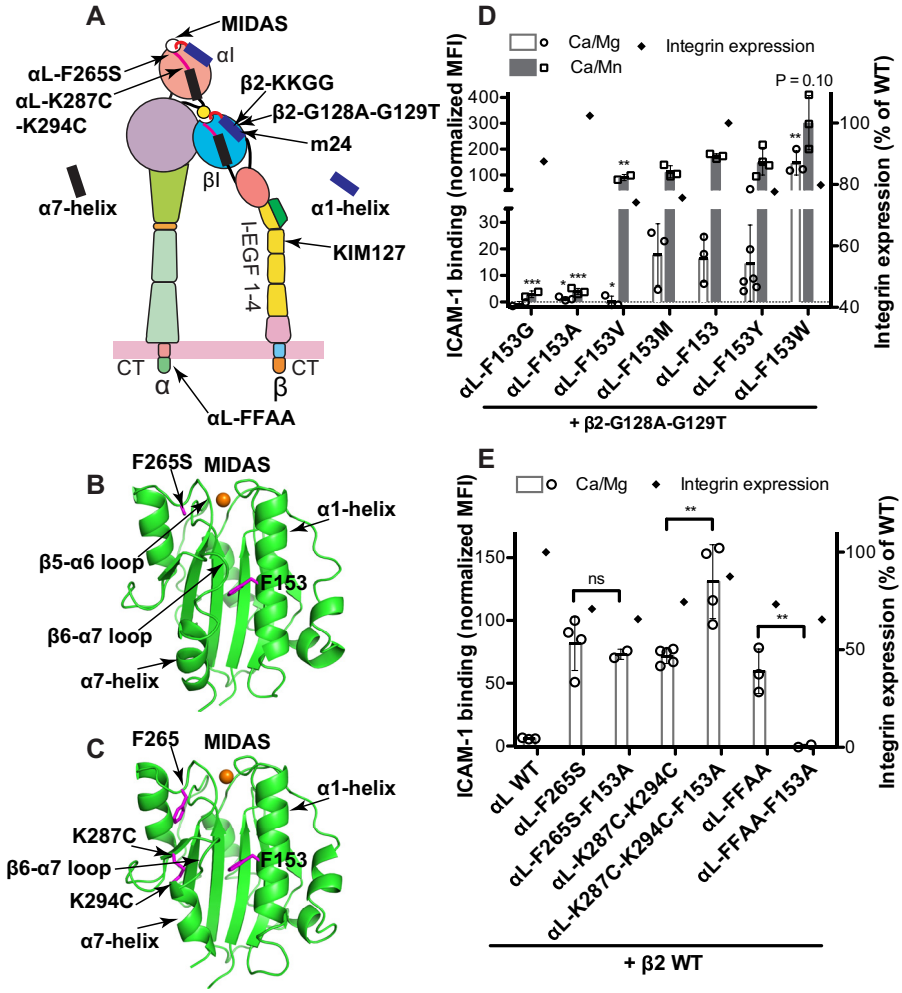


**Figure 3. The combined effect of the $\alpha_L$-Phe-153 mutations and the active $\alpha_L$ or $\beta_2$ mutations on $\alpha_L\beta_2$ ligand binding.** *A*, model of $\alpha_L\beta_2$ integrin at the extended open headpiece conformation. The locations of the indicated mutations and the epitopes of mAbs m24 and KIM127 are shown. *B*, crystal structure of the $\alpha_L$ αI domain with the active F265S mutation (PDB code 3TCX). *C*, crystal structure of the $\alpha_L$ αI domain with the K287C and K294C mutations (PDB code 1T0P). The MIDAS $Mg^{2+}$ ions are shown as *orange spheres*. The side chains of selected residues are shown as *sticks*. *D*, ICAM-1 binding of the HEK293FT cells transfected with the indicated $\alpha_L$-Phe-153 mutants and the active $\beta_2$-G128A/G129T mutant. *E*, ICAM-1 binding of the HEK293FT cells transfected with $\beta_2$ wild type and the $\alpha_L$ subunits having the $\alpha_L$-F153A mutation combined with the active $\alpha_L$-F265S, $\alpha_L$-K287C/K294C or $\alpha_L$-FFAA mutation. The ICAM-1 binding was measured by flow cytometry in the presence of 1 mM $Ca^{2+}/Mg^{2+}$ (*Ca/Mg*) or 0.2 mM $Ca^{2+}$ plus 2 mM $Mn^{2+}$ (*Ca/Mn*) and presented as the MFI normalized to integrin expression. The data are means ± S.D. ($n \geq 3$; for αL-F153G, $n = 2$). Two-tailed *t* tests were used to compare the wild type and the mutants in the same conditions or as indicated. *, $p < 0.05$; **, $p < 0.01$; ***, $p < 0.001$; *ns*, $p > 0.05$. Only the mean values are shown for the integrin expression.

important in $\alpha_L\beta_2$-mediated cell adhesion and spreading on immobilized ICAM-1, given that the receptor-ligand binding kinetics could be different in solution and in the solid phase. When seeded onto the ICAM-1-coated dish, the HEK293FT cells transfected with wild-type $\alpha_L\beta_2$ or $\alpha_L$-F153Y/$\beta_2$ integrin spontaneously adhered and spread on the surface (Fig. 5*A*). However, the $\alpha_L$-F153A mutation completely abolished cell adhesion under the tested coating concentration of ICAM-1 (Fig. 5*A*), despite its comparable cell surface expression with the wild type (Fig. 5*B*). This is in agreement with the pivotal role of the bulky residue of $\alpha_L$-F153 in the high-affinity ligand binding of $\alpha_L\beta_2$.

### *The $\alpha_M$-F156A mutation reduces $\alpha_M\beta_2$-mediated cell adhesion on immobilized fibrinogen*

We next tested whether the conserved Phe residue plays the same role in $\alpha_M$ (Mac-1) integrin that binds multiple ligands including fibrinogen. The $\alpha_M$-Phe-156 was mutated to the small amino acid Ala and the bulky amino acid Trp. The $\alpha_M\beta_2$-mediated cell adhesion on immobilized human fibrinogen was induced by $Mn^{2+}$ ions. The $\alpha_M$-F156A mutation significantly reduced the $\alpha_M\beta_2$-mediated cell adhesion (Fig. 6*A*). By contrast, the bulky $\alpha_M$-F156W mutation significantly enhanced the cell adhesion (Fig. 6*A*). This is not due to the differences in the cell surface expression of $\alpha_M\beta_2$ because both the $\alpha_M$-F156A and $\alpha_M$-F156W mutations decreased the $\alpha_M\beta_2$ expression to a similar extent compared with the wild type (Fig. 6*B*). In addition, the cell adhesion could be blocked by the anti-$\alpha_M$ inhibitory mAb ICRF44 (data not shown). These data demonstrated that a bulky residue is also required for the α1-helix of the $\alpha_M$ αI domain to support ligand binding.

### *Molecular dynamics simulations suggest a structural role of the bulky Phe residue of the αI α1-helix in maintaining the high affinity conformation*

Our experimental data demonstrated an important role of the conserved Phe in the α1-helix of $\alpha_L$ αI domain in high-

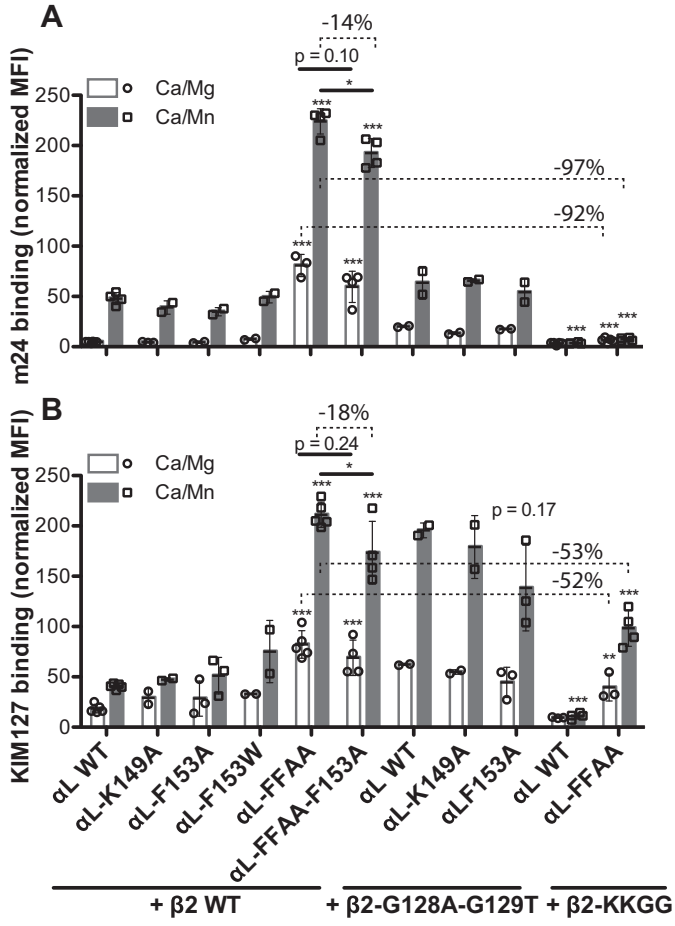


**Figure 4. Effect of the αI α1-helix mutations on $\alpha_L\beta_2$ conformational change.** HEK293FT cells were transfected with the indicated combination of $\alpha_L$ and $\beta_2$ constructs. The cells were incubated with mAb m24 (*A*) that reports $\alpha_L\beta_2$ headpiece opening or KIM127 (*B*) that reports $\alpha_L\beta_2$ extension in the presence of 1 mM $Ca^{2+}/Mg^{2+}$ (*Ca/Mg*) or 0.2 mM $Ca^{2+}$ plus 2 mM $Mn^{2+}$ (*Ca/Mn*). The mAb binding was measured by flow cytometry and presented as the MFI normalized to $\alpha_L\beta_2$ expression measured by TS2/4 binding. The data are means ± S.D. ($n \geq 3$; except for αL-K149A and αL-F153W, $n = 2$). Two-tailed *t* tests were used to compare the wild type and the mutants in the same conditions or as indicated. *, $p < 0.05$; **, $p < 0.01$; ***, $p < 0.001$. The numbers of percentages indicate the decreased levels of mAb binding.

affinity ligand binding. To gain a structural insight into how the Phe affects the conformation of αI domain, we performed the all-atom molecular dynamics (MD) simulation for wild-type and mutant αI domains in water solvent. We used the crystal structure of $\alpha_L$ αI domain in the open conformation for the MD simulation in line with our hypothesis that the bulky Phe may stabilize the active conformation, whereas a small amino acid substitution like Ala would have the opposite effect. A 60-ns MD simulation was performed for both $\alpha_L$ wild type and $\alpha_L$-F153A mutant using exactly the same parameters. To analyze the overall structural similarity of the recorded snapshots to the starting structure, the root mean square deviations (RMSDs) of backbone atoms were calculated. The $\alpha_L$ wild type showed stable RMSD values over the 60-ns simulation. However, the RMSD values of the $\alpha_L$-F153A increased substantially after the first 30-ns simulation, indicating the structure instability (data not shown). To evaluate the conformational dynamics for each residue, we calculated the root mean square fluctuation (RMSF, *i.e.* standard deviation) of Cα positions in the snapshots relative to the starting structure. As shown in Fig. 7*A*, most of the residues of the wild-type $\alpha_L$ αI domain are relatively stable over the 60-ns simulation. Remarkably, in the presence of F153A mutation, the regions of β5-α6 and β6-α7 loops showed significant fluctuations (Fig. 7*A*). These differences became more obvious when the RMSF values were converted to B-factors and represented as cartoon models (Fig. 7*B*). We next performed the same MD simulations for the open-conformation crystal structure of $\alpha_M$ αI domain. The simulation time was extended to 100 ns. Similar to $\alpha_L$-F153A, the $\alpha_M$-F156A mutation rendered the β5-α6 and β6-α7 loops more flexible than the wild type (Fig. 7, *C* and *D*), although to a lesser extent compared with the $\alpha_L$ αI domain (Fig. 7, *A*–*D*). These data clearly demonstrated that the bulky Phe residue of α1-helix contributes to the high affinity state of αI domain by stabilizing the active conformation of β5-α6 and β6-α7 loops.

## Discussion

Integrin is an excellent example of protein machinery in which local conformational changes in one site are propagated to a distal site, altering the ligand-binding affinity and function. Structure-based mutagenesis studies have determined certain residues that are critical for the ligand-binding activity of βI and αI domains (19, 22, 24, 30, 31). Most of the studies focused on the residues that either directly participate in the coordination with the metal ion and/or ligand or that are involved in the movements of the loops or α-helixes surrounding the active site. The importance of these residues is obvious according to the structural changes because the gain-of-function mutations are predicted to shift the conformation to the open state, whereas the loss-of-function mutations are predicted to shift it to the closed state (15, 19, 24). However, a functional role of the conserved Phe of αI α1-helix is unpredictable because this residue seems not directly participate in the movement of either α1-helix or α7-helix based on the structural comparison between the active and inactive conformations. Thus, our findings of the loss-of-function mutation of $\alpha_L$-Phe-153 are unexpected. Our current study further advanced our understanding of the conformational requirement for integrin ligand binding.

How does the $\alpha_L$-Phe-153 contribute to the ligand binding of $\alpha_L$ αI domain? It has been indicated that the downward movement of α7-helix is required for the high affinity ligand binding of αI domain because mutations constraining it at the upward position blocked, whereas mutations facilitating the downward movement enhanced ligand binding (22, 23). In addition, small molecule inhibitors bound to the cavity under the α7-helix allosterically block ligand binding of $\alpha_L\beta_2$ by restraining the downward movement of α7-helix (32–37). Our mutagenesis study showed that the function of a residue at the position of $\alpha_L$-Phe-153 is determined by its size (or volume). A bulky residue is specifically required to maintain the ligand-binding capability of αI domain. At the downward position, the β6-α7 loop moves close to the middle of α1-helix (Figs. 1*I* and 3, *B* and *C*), where a hydrophobic and bulky side chain would act as a pawl to anchor the downward position of β6-α7 loop and α7-helix during their ratchet-like movement (15). This was indicated by the MD simulation data showing that the $\alpha_L$-F153A or $\alpha_M$-F156A mutation rendered the β5-α6 and

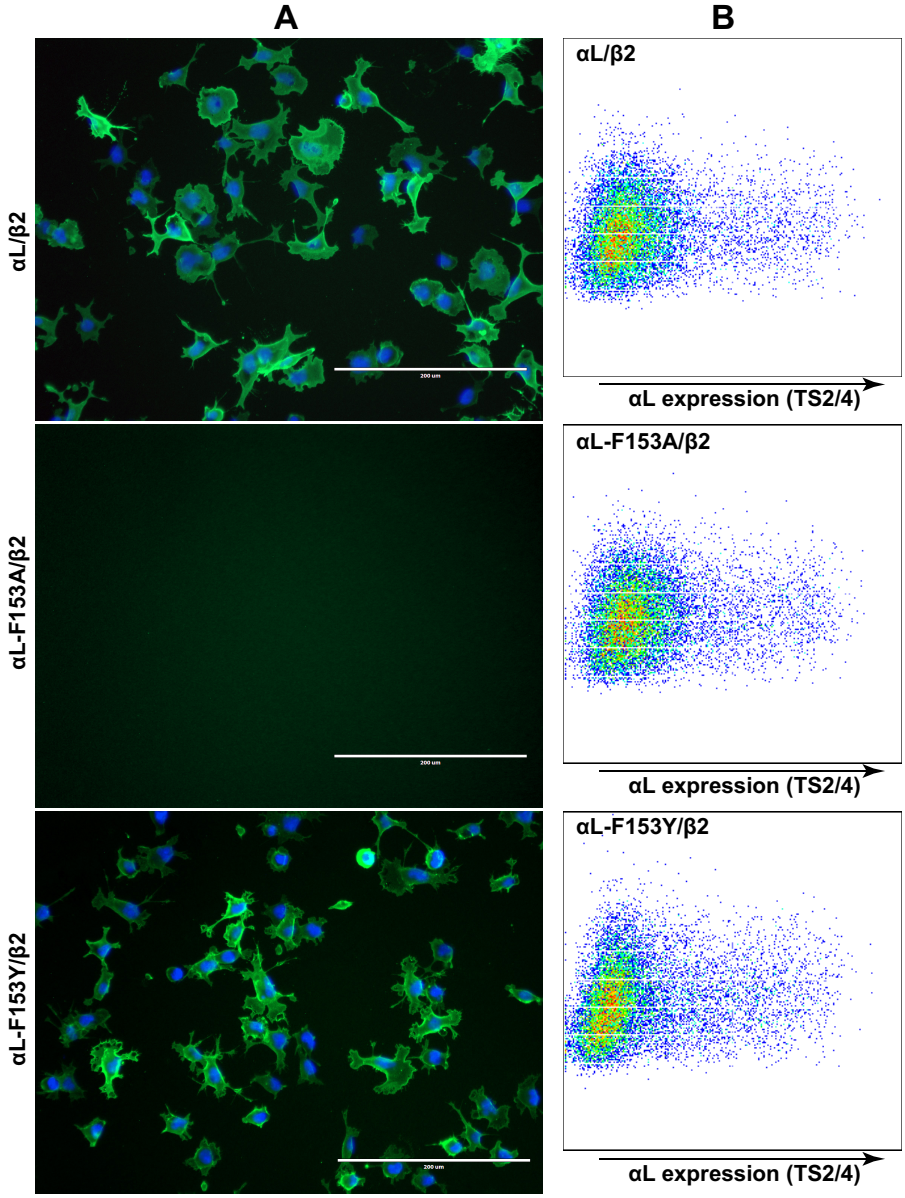


**Figure 5. Effect of $\alpha_L$-Phe-153 mutations on $\alpha_L\beta_2$-mediated cell adhesion and spreading.** *A*, HEK293FT cells transfected with the indicated integrin $\alpha_L\beta_2$ constructs were seeded onto the plates coated with human ICAM-1-Fc (5 $\mu$g/ml coating concentration) at 37 °C for 1 h. The cells were fixed and immunostained with anti-$\alpha_L$ mAb TS2/4 shown in *green*. The nuclei were stained with DAPI. *Scale bar*, 200 $\mu$m. *B*, flow cytometry plots showing integrin $\alpha_L\beta_2$ expression reported by mAb TS2/4 in the corresponding HEK293FT transfectants used in *A*. One representative experiment of more than three repeats is shown.

$\beta$6-$\alpha$7 loops less stable in the active conformation (Fig. 7). The bulky $\alpha_L$-Phe-153 is solely required for the downward movement of $\beta$6-$\alpha$7 loop and $\alpha$7-helix but dispensable for the inward movement of $\alpha$1-helix because once the $\beta$6-$\alpha$7 loop is enforced to the downward position, the trimmed $\alpha$1-helix by the $\alpha_L$-F153A mutation still supports ligand binding. Crystal structures revealed the flexibility of $\alpha$7-helix C terminus both in the isolated form of $\alpha$I domain and in the context of integrin ectodomain (38–41), indicating that the $\alpha$7-helix and the connecting $\beta$6-$\alpha$7 loop can sample rapidly between the closed and the open conformational states. We did not observe the $\beta$6-$\alpha$7 loop and $\alpha$7-helix moving upward to the closed conformation in our MD simulation even in the presence of $\alpha_L$-F153A mutation. This is very likely due to the short time scale used for the simulation. Such a large conformational change may require much longer time of simulation to be observed. Indeed, the hydrogen-deuterium exchange kinetics measured via NMR revealed a large conformational fluctuation of $\alpha$7- but not $\alpha$1-helix in the resting state of the $\alpha_1$ integrin $\alpha$I domain (42). The conserved bulky residue in the middle of $\alpha$1-helix is critical to regulate the shifting between the two states of $\alpha$7-helix by facilitating the transition of the $\alpha$I domain to the high affinity conformation.

It should be noted that although Leu and Met have very close side chain volumes, the $\alpha_L$-F153L mutation exerted a similar level of ICAM-1 binding as the $\alpha_L$ WT, whereas the $\alpha_L$-F153M mutation greatly reduced ICAM-1 binding (Fig. 2*C*). This is consistent with the numbers of rotamers that Leu and Met have. Leu can only sample four rotamer conformations, which is likely to stabilize the downward position of $\beta$6-$\alpha$7 loop and $\alpha$7-helix. In contrast, Met is more flexible by having more than

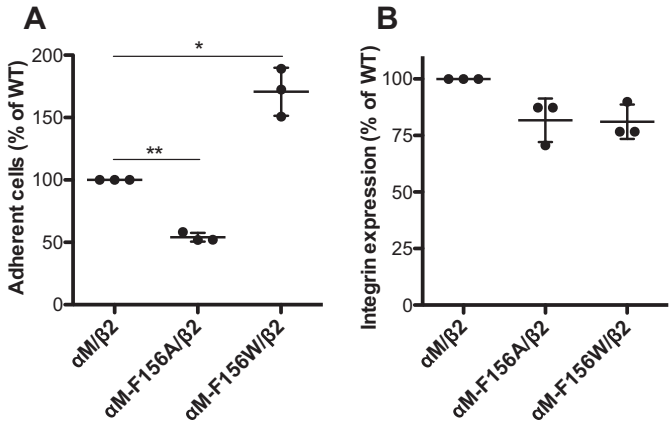


**Figure 6. Effect of the $\alpha_M$-Phe-156 mutations on $\alpha_M\beta_2$-mediated cell adhesion.** *A*, cell adhesion on immobilized human fibrinogen. HEK293FT cells transfected with indicated $\alpha_M\beta_2$ constructs and EGFP were washed with HEPES buffer and then seeded onto the 12-well cell culture plate that was precoated with 3 mg/ml human fibrinogen. The cells were incubated in the presence of 0.2 mM $Ca^{2+}$ plus 2 mM $Mn^{2+}$ at 37 °C for 1 h before washing and fixation. More than 20 images were randomly taken for each sample. The number of EGFP-positive adherent cells was counted for each image and averaged. The cell numbers were normalized to the wild-type level for each independent experiment. *B*, cell surface expression of $\alpha_M\beta_2$ in the same HEK293FT transfectants used for the cell adhesion assay in *A*. The cells were stained with APC-labeled anti-$\alpha_M$ mAb ICRF44, and the mAb binding was measured by flow cytometry. The EGFP-positive cells were acquired for calculating the MFI of APC-ICRF44. The data are presented as percentages of the MFI of $\alpha_M\beta_2$ wild type. The data are means ± S.D. ($n = 3$). Two-tailed *t* tests were used to compare the wild type and the mutants. *, $p < 0.05$; **, $p < 0.01$.

ten rotamer conformations, one of which may adapt to the free movements of β6-α7 loop and α7-helix and thus lack the activation supporting function.

The βI and αI domains are the best-studied VWA domains that undergo conformational changes for affinity regulation. Although their β6-α7 loops and α7-helixes move in a similar fashion to accommodate for the active position of MIDAS loop and to communicate with the neighboring domains, their α1-helixes change in a different fashion (Fig. 1, *H* and *I*). This is in accordance with a conserved Gly and a conserved Phe at the homologous position of α1-helix, which play opposite roles in the βI and αI domains. As we found for a conserved negative role of the Gly in the βI α1-helix (19), the positive role of the Phe in the αI α1-helix could also be generalized to all the αI-containing integrins, given that the same conformational changes of α1- and α7-helix have been observed in the crystal structures of the αI domains of $\alpha_L$, $\alpha_M$, $\alpha_X$, $\alpha_1$, and $\alpha_2$ integrins (12–15, 40, 43, 44). This was demonstrated in the current study on $\alpha_L$ and $\alpha_M$ integrins. Interestingly, an equivalent Phe but not Gly is also present in the α1-helix of many VWA domains other than integrins (Fig. 1*J*). Moreover, most of the VWA domains have only one or lack an intact MIDAS, whereas the integrin βI domains have three metal ion-binding sites that regulate ligand binding. Given the different structural features and conformational regulations of βI domains, it is tempting to speculate that the βI domains might be evolved differently from a typical VWA domain and could be classified as VWA variants.

Although a conserved Phe residue at the equivalent position of αI α1-helix is found in many non-integrin VWA domains, generalizations for the similar function of this residue as seen in the αI domains can only be made with caution. For example, the VWF A1, A2, and A3 domains and the collagen VI α3N5 domain all have an equivalent Phe at the α1-helix, but they lack an intact MIDAS (Fig. 1*J*), and no conformational changes were observed in their α1- and α7-helixes (45–49). Similarly, the presence of an intact MIDAS does not seem to correlate with the presence of the equivalent Phe in the α1-helix. Several examples are found in the complement components C2a and factor B, in the thrombospondin repeat anonymous proteins (TRAPs) of the *Plasmodium vivax* and *Plasmodium falciparum*, and in the pilus-related adhesion RrgA of *Streptococcus pneumoniae*, in which a non-Phe residue is present at the equivalent position of α1-helix (Fig. 1*J*). We compared the crystal structures of several representative VWA domains that have an intact MIDAS, which has been suggested or confirmed to participate in ligand binding (Fig. 8). Crystal structures of the VWA domain of human anthrax toxin receptor 2 (ANTR2) in complex with anthrax toxin or pseudo-ligands highly resemble the active open conformation of integrin αI domain (Fig. 8*A*) (50). Although a closed conformation has yet to be seen for the ANTR2 VWA domain, mutagenesis studies suggested that it might undergo conformational changes for affinity regulation and signaling (51). Other VWA domains that have similar conformational regulations as integrin αI domains are from the adhesins of the parasites *Toxoplasma gondii* micronemal protein 2 (TgMIC2) and the *P. vivax* TRAP or *P. falciparum* TRAP as mentioned above. The TRAP VWA domain has been seen in both the closed and open conformations (Fig. 8*B*) (52). The MIC2 VWA domain has only been crystalized in the closed conformation so far (Fig. 8*C*), but the transition between the closed and the open states is highly predictable (53). A recent crystal structure of the Blue Mussels adhesion protein, the PTMP1 (proximal thread matrix protein 1) revealed two tandem VWA domains both in the closed conformation with the A1 domain MIDAS occupied by $Zn^{2+}$ (Fig. 8*D*) (54). It was suggested that the MIDAS of PTMP1 might participate in collagen binding (54), which resembles the interaction of the $\alpha_2$ integrin αI domain and collagen. All the above-mentioned VWA domains contain the equivalent Phe at the α1-helix except that some TRAP proteins have a Leu or Met (Figs. 1*J* and 8, *A–D*). However, our data showed that a Met or Leu residue at the equivalent position of α1-helix could still support the ligand binding of αI domain (Figs. 2*C* and 3*D*). Therefore, it is tempting to speculate that these VWA domains may follow the activating mechanism of integrin αI domains.

We presented two examples of VWA domains from the bacteria adhesin RrgA (Fig. 8*E*) (55) and the complement factor B (Fig. 8*F*) (56), which have a small amino acid at the equivalent position of α1-helix. The crystal structure of RrgA VWA domain shows a closed conformation of MIDAS and α7-helix and an Ala at the Phe-equivalent position of α1-helix (Fig. 8*E*). Notably, the loop connecting the MIDAS motif and the α1-helix in RrgA is much longer than that of $\alpha_L$ αI domain (Figs. 1*J* and 8*E*). This longer MIDAS loop may move freely toward the metal ion to accommodate with the high affinity ligand binding even without the inward movement of the α1-helix and the downward movement of the α7-helix. As such, a bulky residue in the mid α1-helix is not essential. The VWA domain of complement factor B was crystallized in both the closed and open

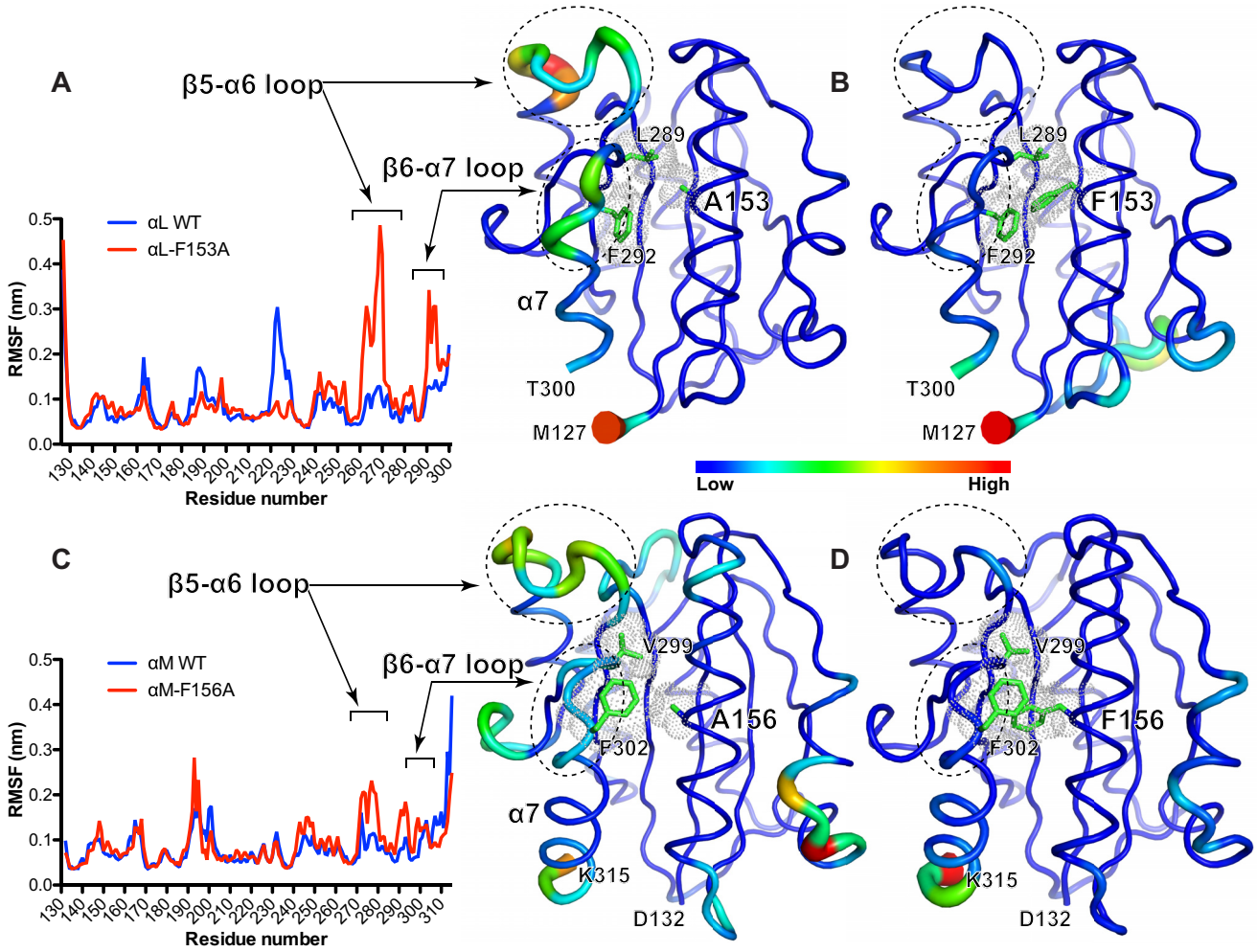


**Figure 7. Molecular dynamics simulations of the $\alpha_L$ and $\alpha_M$ αI domains.** *A*, RMSF of the Cα positions in a 60-ns MD simulation of the αI domain of $\alpha_L$ WT or $\alpha_L$-F153A mutant in the open conformation. *B*, cartoon models of the open $\alpha_L$ αI domains with Ala-153 and Phe-153. *C*, RMSF of the Cα positions in a 100-ns MD simulation of the αI domain of $\alpha_M$ WT or $\alpha_M$-F156A mutant in the open conformation. *D*, cartoon models of the open $\alpha_M$ αI domains with Ala-156 and Phe-156. To indicate the fluctuations of the Cα atoms, the RMSF values in the plots were converted to B-factor values and shown in the cartoon models with the Cα color and cartoon putty scaled based on the B-factors. The regions of interest are *circled* in the cartoons and indicated in the RMSF plots. The residues of interest are shown as *green sticks* with the *dots* representing van der Waals surface.

conformations (56, 57). It has a Cys at the equivalent position of α1-helix (Figs. 1*J* and 8*F*). Although there is a swung-in motion at the N terminus of α1-helix, the scale of the downward movement of α7-helix is very small in the open conformation (Fig. 8*F*). The movement of α7-helix seems to be induced by the binding of factor D (56). In addition, the factor B VWA domain has an extra αL-helix, which interacts with the α7-helix and influences its conformation (Fig. 8*F*). All these differences may minimize the requirement of a bulky residue at the α1-helix. In summary, our study revealed a unique feature of integrin αI α1-helix in regulating ligand binding, which may be applicable to certain VWA domains of other proteins that undergo large conformational changes for signal transduction.

Another important finding in the current study is that integrin conformational transmission can be uncoupled between the αI and the βI domains. We found that although the conserved Phe of α1-helix is critical for ICAM-1 binding to αI domain, it is dispensable for $\beta_2$ extension and headpiece opening. The downward displacement of α7-helix that requires the Phe of α1-helix is not essential for the conformational changes of $\beta_2$ induced by $Mn^{2+}$ or by inside-out activation. In addition, previous studies also showed that locking the downward conformation of α7-helix of αI domain did not result in $\beta_2$ extension or headpiece opening (22). Interestingly, the internal ligand $\alpha_L$-Glu-310 at the C terminus of α7-helix is required for the headpiece opening of $\beta_2$ subunit (58). Recent crystal structures of $\alpha_X\beta_2$ and $\alpha_L\beta_2$ suggested the intrinsic flexibility of αI domain on the platform formed by the β-propeller and βI domains (39–41). This is consistent with the loose conformational linkage between the βI and αI domains. The $\alpha_L\beta_2$ integrin mediates both the rolling adhesion and migration of leukocytes by binding the ICAM-1 expressed on the endothelial cells (59). Under the rolling condition, the loose linkage between the αI and βI enables the cells to quickly bind and release ICAM-1. When the cell signals for firm adhesion and migration are turned on, the tight engagement of the αI and βI domains could be enforced by the mechanical forces generated by the actin polymerization and ICAM-1 binding at each end of integrin (60).

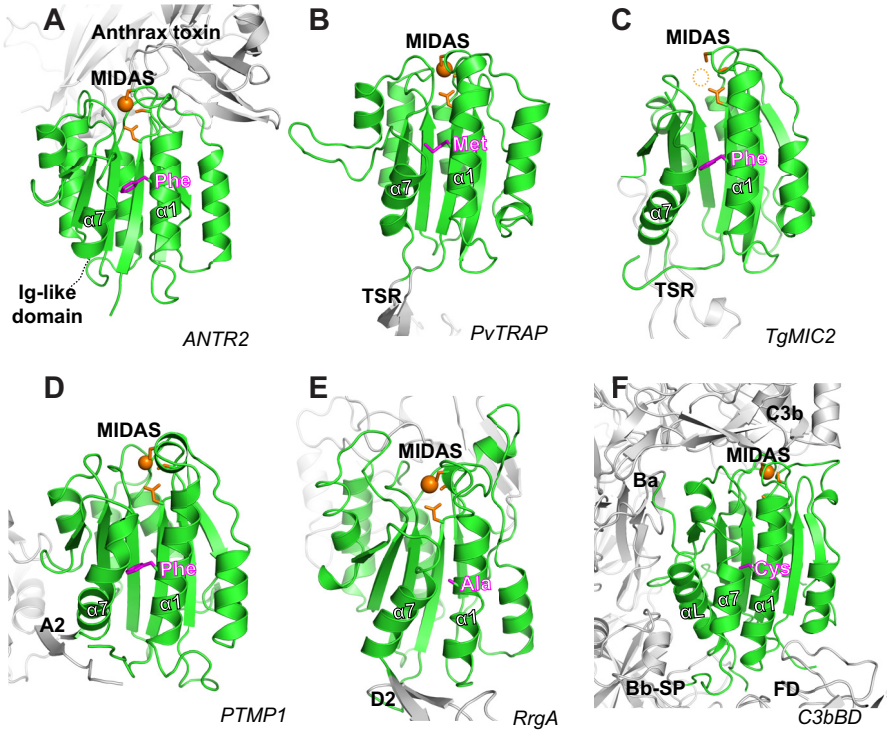


**Figure 8. Representative VWA structures.** *A–F*, the crystal structures of VWA domains (in *green*) of human anthrax toxin receptor 2 bound with anthrax toxin (PDB code 1T6B) (*A*); *P. vivax* thrombospondin repeat anonymous protein (PDB code 4HQL) (*B*); *T. gondii* micronemal protein 2 (PDB code 4OKR) (*C*); blue mussel proximal thread matrix protein 1 (PDB code 4CN9) (*D*); *S. pneumoniae* pilus-related adhesion, RrgA (PDB code 2WW8) (*E*); and human complement C3b bound with factor B and factor D (PDB code 2XWB) (*F*). The D*XSXS* motif and metal ions of MIDAS are shown in *orange*. The residues of α1-helix that are equivalent to the Phe of integrin αI α1-helix are shown in *magenta*.

## Experimental procedures

### *DNA constructs*

DNA constructs of human $\alpha_L$ and $\beta_2$ integrins were as described previously (19). The full-length cDNA of human $\alpha_M$ integrin was cloned into the pcDNA3.1 vector using the 5-′ KpnI and 3-′ XbaI sites. Mutations were introduced by site-directed mutagenesis with the QuikChange kit (Agilent Technologies).

### *Antibodies and protein ligands*

TS2/4 (BioLegend) is a non-functional anti-$\alpha_L$ mAb (61). KIM127 (binds to I-EGF2 domain) and mAb 24 (m24, binds to βI domain) are anti-$\beta_2$ conformation-specific mAbs that report $\beta_2$ integrin extension and headpiece opening, respectively (27, 29, 62, 63). ICRF44 (BioLegend) is an inhibitory anti-$\alpha_M$ mAb. Human ICAM-1 (with a C-terminal tag of human IgG1 Fc, ICAM-1-Fc) was purchased from Sino Biological. Biotin-labeled mouse anti-human IgG1 Fc, Alexa Fluor 488-conjugated goat anti-mouse IgG, and Alexa Fluor 647-conjugated streptavidin were from ThermoFisher Scientific.

### *Soluble ligand-binding assay*

HEK293FT cells (ThermoFisher Scientific) were cultured in DMEM plus 10% FBS at 37 °C with 5% $CO_2$. ICAM-1 binding of HEK293FT cells was as described before (19, 21). The cells were co-transfected with $\alpha_L$ and $\beta_2$ integrin constructs with Lipofectamine 2000 (ThermoFisher Scientific) for at least 24 h. Transfected cells were incubated in HBSGB buffer (20 mM HEPES, pH 7.4, 150 mM NaCl, 5.5 mM glucose, and 1% BSA) with 15 μg/ml each of ICAM-1-Fc and biotin-labeled mouse anti-human IgG1 Fc in the presence of 5 mM EDTA or 1 mM $Ca^{2+}/Mg^{2+}$ or 0.2 mM $Ca^{2+}$ plus 2 mM $Mn^{2+}$ at 25 °C for 30 min. The cells were then washed and incubated on ice for 30 min with 10 μg/ml FITC-labeled TS2/4 and 10 μg/ml Alexa Fluor 647-labeled streptavidin. TS2/4-positive cells (expressing $\alpha_L\beta_2$ integrin) were acquired for calculating the mean fluorescence intensity (MFI) by flow cytometry using BD Accuri™ C6 flow cytometer. ICAM-1 binding was presented as normalized MFI, *i.e.* ICAM-1 MFI (after subtracting the ICAM-1 MFI in the EDTA condition) as a percentage of TS2/4 MFI (integrin expression).

### *Conformation-specific antibody binding*

Binding of the active conformation-specific anti-$\beta_2$ mAbs KIM127 and m24 to the HEK293FT transfectants was performed as described before (19, 21). In brief, the cells were first incubated with 10 μg/ml biotin-labeled KIM127 or m24 in HBSGB buffer containing 1 mM $Ca^{2+}/Mg^{2+}$ or 0.2 mM $Ca^{2+}$ plus 2 mM $Mn^{2+}$ at 25 °C for 30 min and then washed and incubated with 10 μg/ml FITC-labeled TS2/4 and Alexa Fluor 647-labeled streptavidin on ice for 30 min. TS2/4-positive cells were acquired for calculating the MFI by flow cytometry. The KIM127 or m24 binding was presented as normalized MFI, *i.e.* streptavidin MFI as a percentage of TS2/4 MFI.

### *Cell adhesion assay and fluorescence microscopy*

For $\alpha_L\beta_2$-mediated cell adhesion assay, the Delta T dishes (Bioptechs) or 24-well cell culture plate (BD Falcon) were first

coated with 5 μg/ml mouse anti-human IgG in pH 7.4, PBS, at 4 °C for 12 h, and then blocked with 1% BSA at 37 °C for 1 h before finally coated with 5 μg/ml ICAM-1-Fc at 37 °C for another 1 h. Transfected HEK293FT cells suspended in DMEM without FBS were allowed to adhere on the ICAM-1-Fc-coated Delta T dishes at 37 °C for 1 h. The unattached cells were washed off by DMEM, and the attached cells were fixed with DMEM containing 3.7% formaldehyde, blocked with 5% nonfat dry milk in PBS, and stained with 10 μg/ml mAb TS2/4 and Alexa Fluor 488-labeled goat anti-mouse IgG. The nuclei were stained with 5 μg/ml DAPI. The stained cells were fixed with 3.7% formaldehyde in PBS and imaged with an EVOS digital inverted fluorescence microscope with a 20× objective. The level of integrin expression of the transfected cells was accessed by the mAb TS2/4 staining, followed by flow cytometry.

For $\alpha_M\beta_2$-mediated cell adhesion assay, the 12-well cell culture plate was coated with 3 mg/ml human fibrinogen in PBS at 37 °C for 1 h. HEK293FT cells transfected with $\alpha_M\beta_2$ plus EGFP were seeded onto the fibrinogen-coated plate in HEPES buffer for 10 min before adding 0.2 mM $Ca^{2+}$ plus 2 mM $Mn^{2+}$. After incubation at 37 °C for 1 h, the plate was washed with PBS buffer for three times and fixed with 3.7% formaldehyde in PBS. The adhered cells were imaged with an EVOS digital inverted fluorescence microscope with a 10× objective. At least 20 images were randomly taken for each sample, and the EGFP-positive cells were counted for each image. The data were presented as the averaged cell numbers that were normalized to the WT level. The cell surface expression of $\alpha_M\beta_2$ was measured by flow cytometry after staining with the allophycocyanin (APC)-labeled anti-$\alpha_M$ mAb ICRF44 (BioLegend).

### *Molecular dynamics simulation*

The crystal structures of the $\alpha_L$ αI (PDB code 1T0P) and the $\alpha_M$ αI domains (PDB code 1IDO) in the open conformation were used for MD simulation. $\alpha_L$-Phe-153 and $\alpha_M$-Phe-156 were mutated to Ala *in silico* using PyMOL. For the $\alpha_L$ αI structure (PDB code 1T0P), the two cysteine mutations, K287C and K294C, were mutated back to their native Lys residue by PyMOL to remove the engineered disulfide-bond that was used to stabilize the open conformation of β6-α7 loop and α7-helix. GROMACS version 2016.3 was used to prepare the structures and perform the production MD simulation using the OPLS-AA/L all-atom force field (64, 65). The protein was centered in a cubic box with a minimum distance to any wall of 1.2 nm. The box was filled with TIP3 water model and 100 mM NaCl. Energy minimization and equilibrations of temperature and pressure were performed before conducting the unrestrained 60- or 100-ns production MD simulation. The RMSDs and RMSFs of the backbone or Cα atoms were calculated for the recorded trajectories to evaluate the stability of the conformations.

### *Statistical analysis*

The two-tailed Student's *t* test was performed using the GraphPad Prism software to calculate the *p* values for comparing the data between two experimental groups.

*Author contributions*—Z. W. and A. M. M. T. performed the experiments and analyzed the data. J. Z. designed the study, analyzed data, and wrote the manuscript. All authors contributed to the manuscript preparation.

*Acknowledgments—We thank Drs. Chafen Lu and Timothy Springer for providing antibodies.*

**References**


1. Hynes, R. O. (2002) Integrins: bi-directional, allosteric, signalling machines. *Cell* **110,** 673–687
2. Iwamoto, D. V., and Calderwood, D. A. (2015) Regulation of integrin-mediated adhesions. *Curr. Opin. Cell Biol.* **36,** 41–47
3. Sun, Z., Guo, S. S., and Fässler, R. (2016) Integrin-mediated mechanotransduction. *J. Cell Biol.* **215,** 445–456
4. Humphrey, J. D., Dufresne, E. R., and Schwartz, M. A. (2014) Mechanotransduction and extracellular matrix homeostasis. *Nat. Rev. Mol. Cell Biol.* **15,** 802–812
5. Springer, T. A., and Dustin, M. L. (2012) Integrin inside-out signaling and the immunological synapse. *Curr. Opin. Cell Biol.* **24,** 107–115
6. Takagi, J., and Springer, T. A. (2002) Integrin activation and structural rearrangement. *Immunol. Rev.* **186,** 141–163
7. Arnaout, M. A., Mahalingam, B., and Xiong, J. P. (2005) Integrin structure, allostery, and bidirectional signaling. *Annu. Rev. Cell Dev. Biol.* **21,** 381–410
8. Kim, C., Ye, F., and Ginsberg, M. H. (2011) Regulation of integrin activation. *Annu. Rev. Cell Dev. Biol.* **27,** 321–345
9. Shattil, S. J., Kim, C., and Ginsberg, M. H. (2010) The final steps of integrin activation: the end game. *Nat. Rev. Mol. Cell Biol.* **11,** 288–300
10. Liddington, R. C. (2014) Structural aspects of integrins. *Adv. Exp. Med. Biol.* **819,** 111–126
11. Luo, B.-H., Carman, C. V., and Springer, T. A. (2007) Structural basis of integrin regulation and signaling. *Annu. Rev. Immunol.* **25,** 619–647
12. Lee, J.-O., Bankston, L. A., Arnaout, M. A., and Liddington, R. C. (1995) Two conformations of the integrin A-domain (I-domain): a pathway for activation? *Structure* **3,** 1333–1340
13. Lee, J.-O., Rieu, P., Arnaout, M. A., and Liddington, R. (1995) Crystal structure of the A domain from the α subunit of integrin CR3 (CD11b/CD18). *Cell* **80,** 631–638
14. Emsley, J., Knight, C. G., Farndale, R. W., Barnes, M. J., and Liddington, R. C. (2000) Structural basis of collagen recognition by integrin $\alpha_2\beta_1$. *Cell* **101,** 47–56
15. Shimaoka, M., Xiao, T., Liu, J.-H., Yang, Y., Dong, Y., Jun, C.-D., McCormack, A., Zhang, R., Joachimiak, A., Takagi, J., Wang J.-H., Springer, T. A. (2003) Structures of the $\alpha_L$ I domain and its complex with ICAM-1 reveal a shape-shifting pathway for integrin regulation. *Cell* **112,** 99–111
16. Xiao, T., Takagi, J., Wang, J.-H., Coller, B. S., Springer, T. A. (2004) Structural basis for allostery in integrins and binding of fibrinogen-mimetic therapeutics. *Nature* **432,** 59–67
17. Zhu, J., Zhu, J., and Springer, T. A. (2013) Complete integrin headpiece opening in eight steps. *J. Cell Biol.* **201,** 1053–1068
18. Whittaker, C. A., and Hynes, R. O. (2002) Essay from the genome annotation series: distribution and evolution of the von Willebrand/integrin A domain: a widely dispersed domain with roles in cell adhesion and elsewhere. *Mol. Biol. Cell* **13,** 3369–3387
19. Zhang, C., Liu, J., Jiang, X., Haydar, N., Zhang, C., Shan, H., and Zhu, J. (2013) Modulation of integrin activation and signaling by α1/α1′-helix unbending at the junction. *J. Cell Sci.* **126,** 5735–5747
20. Qu, A., and Leahy, D. J. (1996) The role of the divalent cation in the structure of the I domain from the CD11a/CD18 integrin. *Structure* **4,** 931–942
21. Liu, J., Wang, Z., Thinn, A. M., Ma, Y. Q., and Zhu, J. (2015) The dual structural roles of the membrane distal region of the α-integrin cytoplasmic tail during integrin inside-out activation. *J. Cell Sci.* **128,** 1718–1731
22. Lu, C., Shimaoka, M., Zang, Q., Takagi, J., and Springer, T. A. (2001) Locking in alternate conformations of the integrin $\alpha_L\beta_2$ I domain with disulfide bonds reveals functional relationships among integrin domains. *Proc. Natl. Acad. Sci. U.S.A.* **98,** 2393–2398




ASBMB

23. Shimaoka, M., Lu, C., Salas, A., Xiao, T., Takagi, J., and Springer, T. A. (2002) Stabilizing the integrin $\alpha_M$ inserted domain in alternative conformations with a range of engineered disulfide bonds. *Proc. Natl. Acad. Sci. U.S.A.* **99,** 16737–16741
24. Jin, M., Song, G., Carman, C. V., Kim, Y.-S., Astrof, N. S., Shimaoka, M., Wittrup, D. K., and Springer, T. A. (2006) Directed evolution to probe protein allostery and integrin I domains of 200,000-fold higher affinity. *Proc. Natl. Acad. Sci. U.S.A.* **103,** 5758–5763
25. Lu, C. F., and Springer, T. A. (1997) The α subunit cytoplasmic domain regulates the assembly and adhesiveness of integrin lymphocyte function-associated antigen-1 (LFA-1). *J. Immunol.* **159,** 268–278
26. Humphries, M. J. (2004) Monoclonal antibodies as probes of integrin priming and activation. *Biochem. Soc. Trans.* **32,** 407–411
27. Chen, X., Xie, C., Nishida, N., Li, Z., Walz, T., and Springer, T. A. (2010) Requirement of open headpiece conformation for activation of leukocyte integrin $\alpha_X\beta_2$. *Proc. Natl. Acad. Sci. U.S.A.* **107,** 14727–14732
28. Lu, C., Ferzly, M., Takagi, J., and Springer, T. A. (2001) Epitope mapping of antibodies to the C-terminal region of the integrin $\beta_2$ subunit reveals regions that become exposed upon receptor activation. *J. Immunol.* **166,** 5629–5637
29. Nishida, N., Xie, C., Shimaoka, M., Cheng, Y., Walz, T., and Springer, T. A. (2006) Activation of leukocyte $\beta_2$ integrins by conversion from bent to extended conformations. *Immunity* **25,** 583–594
30. Shimaoka, M., Shifman, J. M., Jing, H., Takagi, J., Mayo, S. L., and Springer, T. A. (2000) Computational design of an integrin I domain stabilized in the open, high affinity conformation. *Nat. Struct. Biol.* **7,** 674–678
31. Barton, S. J., Travis, M. A., Askari, J. A., Buckley, P. A., Craig, S. E., Humphries, M. J., and Mould, A. P. (2004) Novel activating and inactivating mutations in the integrin $\beta_1$ subunit A domain. *Biochem. J.* **380,** 401–407
32. Kallen, J., Welzenbach, K., Ramage, P., Geyl, D., Kriwacki, R., Legge, G., Cottens, S., Weitz-Schmidt, G., and Hommel, U. (1999) Structural basis for LFA-1 inhibition upon lovastatin binding to the CD11a I-domain. *J. Mol. Biol.* **292,** 1–9
33. Crump, M. P., Ceska, T. A., Spyracopoulos, L., Henry, A., Archibald, S. C., Alexander, R., Taylor, R. J., Findlow, S. C., O'Connell, J., Robinson, M. K., and Shock, A. (2004) Structure of an allosteric inhibitor of LFA-1 bound to the I-domain studied by crystallography, NMR, and calorimetry. *Biochemistry* **43,** 2394–2404
34. Weitz-Schmidt, G., Welzenbach, K., Dawson, J., and Kallen, J. (2004) Improved LFA-1 inhibition by statin derivatives: Molecular basis determined by X-ray analysis and monitoring of LFA-1 conformational changes *in vitro* and *ex vivo*. *J. Biol. Chem.* **279,** 46764–46771
35. Wattanasin, S., Kallen, J., Myers, S., Guo, Q., Sabio, M., Ehrhardt, C., Albert, R., Hommel, U., Weckbecker, G., Welzenbach, K., and Weitz-Schmidt, G. (2005) 1,4-Diazepane-2,5-diones as novel inhibitors of LFA-1. *Bioorg. Med. Chem. Lett.* **15,** 1217–1220
36. Potin, D., Launay, M., Monatlik, F., Malabre, P., Fabreguettes, M., Fouquet, A., Maillet, M., Nicolai, E., Dorgeret, L., Chevallier, F., Besse, D., Dufort, M., Caussade, F., Ahmad, S. Z., Stetsko, D. K., *et al.* (2006) Discovery and development of 5-[(5S,9R)-9-(4-cyanophenyl)-3-(3,5-dichlorophenyl)-1-methyl-2,4-dioxo-1,3,7-tria zaspiro[4.4]non-7-yl-methyl]-3-thiophenecarboxylic acid (BMS-587101): a small molecule antagonist of leukocyte function associated antigen-1. *J. Med. Chem.* **49,** 6946–6949
37. Zhang, H., Astrof, N. S., Liu, J. H., Wang, J. H., and Shimaoka, M. (2009) Crystal structure of isoflurane bound to integrin LFA-1 supports a unified mechanism of volatile anesthetic action in the immune and central nervous systems. *FASEB J.* **23,** 2735–2740
38. Zhang, H., Casasnovas, J. M., Jin, M., Liu, J. H., Gahmberg, C. G., Springer, T. A., and Wang, J. H. (2008) An unusual allosteric mobility of the C-terminal helix of a high-affinity $\alpha_L$ integrin I domain variant bound to ICAM-5. *Mol. Cell* **31,** 432–437
39. Xie, C., Zhu, J., Chen, X., Mi, L., Nishida, N., and Springer, T. A. (2010) Structure of an integrin with an α I domain, complement receptor type 4. *EMBO J.* **29,** 666–679
40. Sen, M., Yuki, K., and Springer, T. A. (2013) An internal ligand-bound, metastable state of a leukocyte integrin, $\alpha_X\beta_2$. *J. Cell Biol.* **203,** 629–642
41. Sen, M., and Springer, T. A. (2016) Leukocyte integrin $\alpha_L\beta_2$ headpiece structures: The αI domain, the pocket for the internal ligand, and concerted movements of its loops. *Proc. Natl. Acad. Sci. U.S.A.* **113,** 2940–2945
42. Nunes, A. M., Zhu, J., Jezioro, J., Minetti, C. A., Remeta, D. P., Farndale, R. W., Hamaia, S. W., and Baum, J. (2016) Intrinsic local destabilization of the C-terminus predisposes integrin $\alpha_1$ I domain to a conformational switch induced by collagen binding. *Protein Sci.* **25,** 1672–1681
43. Chin, Y. K., Headey, S. J., Mohanty, B., Patil, R., McEwan, P. A., Swarbrick, J. D., Mulhern, T. D., Emsley, J., Simpson, J. S., and Scanlon, M. J. (2013) The structure of integrin $\alpha_1$ I domain in complex with a collagen-mimetic peptide. *J. Biol. Chem.* **288,** 36796–36809
44. Bajic, G., Yatime, L., Sim, R. B., Vorup-Jensen, T., and Andersen, G. R. (2013) Structural insight on the recognition of surface-bound opsonins by the integrin I domain of complement receptor 3. *Proc. Natl. Acad. Sci. U.S.A.* **110,** 16426–16431
45. Brondijk, T. H., Bihan, D., Farndale, R. W., and Huizinga, E. G. (2012) Implications for collagen I chain registry from the structure of the collagen von Willebrand factor A3 domain complex. *Proc. Natl. Acad. Sci. U.S.A.* **109,** 5253–5258
46. Jakobi, A. J., Mashaghi, A., Tans, S. J., and Huizinga, E. G. (2011) Calcium modulates force sensing by the von Willebrand factor A2 domain. *Nat. Commun.* **2,** 385
47. Zhou, M., Dong, X., Baldauf, C., Chen, H., Zhou, Y., Springer, T. A., Luo, X., Zhong, C., Gräter, F., and Ding, J. (2011) A novel calcium-binding site of von Willebrand factor A2 domain regulates its cleavage by ADAMTS13. *Blood* **117,** 4623–4631
48. Zhang, Q., Zhou, Y.-F., Zhang C.-Z., Zhang, C. Z., Zhang, X., Lu, C., and Springer, T. A. (2009) Structural specializations of A2, a force-sensing domain in the ultralarge vascular protein von Willebrand factor. *Proc. Natl. Acad. Sci. U.S.A.* **106,** 9226–9231
49. Huizinga, E. G., Tsuji, S., Romijn, R. A., Schiphorst, M. E., de Groot, P. G., Sixma, J. J., and Gros, P. (2002) Structures of glycoprotein Ibα and its complex with von Willebrand factor A1 domain. *Science* **297,** 1176–1179
50. Santelli, E., Bankston, L. A., Leppla, S. H., and Liddington, R. C. (2004) Crystal structure of a complex between anthrax toxin and its host cell receptor. *Nature* **430,** 905–908
51. Deuquet, J., Lausch, E., Superti-Furga, A., and van der Goot, F. G. (2012) The dark sides of capillary morphogenesis gene 2. *EMBO J.* **31,** 3–13
52. Song, G., Koksal, A. C., Lu, C., and Springer, T. A. (2012) Shape change in the receptor for gliding motility in *Plasmodium sporozoites*. *Proc. Natl. Acad. Sci. U.S.A.* **109,** 21420–21425
53. Song, G., and Springer, T. A. (2014) Structures of the *Toxoplasma* gliding motility adhesin. *Proc. Natl. Acad. Sci. U.S.A.* **111,** 4862–4867
54. Suhre, M. H., Gertz, M., Steegborn, C., and Scheibel, T. (2014) Structural and functional features of a collagen-binding matrix protein from the mussel byssus. *Nat. Commun.* **5,** 3392
55. Izoré, T., Contreras-Martel, C., El Mortaji, L., Manzano, C., Terrasse, R., Vernet, T., Di Guilmi, A. M., and Dessen, A. (2010) Structural basis of host cell recognition by the pilus adhesin from *Streptococcus pneumoniae*. *Structure* **18,** 106–115
56. Forneris, F., Ricklin, D., Wu, J., Tzekou, A., Wallace, R. S., Lambris, J. D., and Gros, P. (2010) Structures of C3b in complex with factors B and D give insight into complement convertase formation. *Science* **330,** 1816–1820
57. Milder, F. J., Gomes, L., Schouten, A., Janssen, B. J., Huizinga, E. G., Romijn, R. A., Hemrika, W., Roos, A., Daha, M. R., and Gros, P. (2007) Factor B structure provides insights into activation of the central protease of the complement system. *Nat. Struct. Mol. Biol.* **14,** 224–228
58. Salas, A., Shimaoka, M., Kogan, A. N., Harwood, C., von Andrian, U. H., and Springer, T. A. (2004) Rolling adhesion through an extended conformation of integrin $\alpha_L\beta_2$ and relation to α I and β I-like domain interaction. *Immunity* **20,** 393–406
59. Springer, T. A. (1994) Traffic signals for lymphocyte recirculation and leukocyte emigration: the multi-step paradigm. *Cell* **76,** 301–314
60. Nordenfelt, P., Elliott, H. L., and Springer, T. A. (2016) Coordinated integrin activation by actin-dependent force during T-cell migration. *Nat. Commun.* **7,** 13119

61. Sanchez-Madrid, F., Krensky, A. M., Ware, C. F., Robbins, E., Strominger, J. L., Burakoff, S. J., and Springer, T. A. (1982) Three distinct antigens associated with human T lymphocyte-mediated cytolysis: LFA-1, LFA-2, and LFA-3. *Proc. Natl. Acad. Sci. U.S.A.* **79,** 7489–7493
62. Robinson, M. K., Andrew, D., Rosen, H., Brown, D., Ortlepp, S., Stephens, P., and Butcher, E. C. (1992) Antibody against the Leu-cam β-chain (CD18) promotes both LFA-1-and CR3-dependent adhesion events. *J. Immunol.* **148,** 1080–1085
63. Dransfield, I., and Hogg, N. (1989) Regulated expression of $Mg^{2+}$ binding epitope on leukocyte integrin α subunits. *EMBO J.* **8,** 3759–3765
64. Jorgensen, W. L., Maxwell, D. S., and Tirado-Rives, J. (1996) Development and testing of the OPLS all-atom force field on conformational energetics and properties of organic liquids. *J. Am. Chem. Soc.* **118,** 11225–11236
65. Kaminski, G. A., Friesner, R. A., Tirado-Rives, J., and Jorgensen, W. L. (2001) Evaluation and reparametrization of the OPLS-AA force field for proteins via comparison with accurate quantum chemical calculations on peptides. *J. Phys. Chem. B* **105,** 6474–6487
66. Harpaz, Y., Gerstein, M., and Chothia, C. (1994) Volume changes on protein folding. *Structure* **2,** 641–649



ASBMB